sustainability

MDPI

Article

Using the Sentinel-3B Satellite in Geospatial Analysis of Suspended Aerosols in the Kiev, Ukraine Region

Alcindo Neckel [1,*], M. Santosh [2,3], Brian William Bodah [1,4,5], Laércio Stolfo Maculan [1], Diana Pinto [6], Cleiton Korcelski [1], Paloma Carollo Toscan [1], Laura Pasa Cambrussi [1], Isadora Cezar Caino [1], Leila Dal Moro [1], Dirceu Piccinato Junior [1], Grace Tibério Cardoso [1], Caliane Christie Oliveira de Almeida Silva [1] and Giana de Vargas Mores [1]

1 ATITUS Educação, Passo Fundo 99070-220, Brazil
2 School of Earth Sciences and Resources, China University of Geosciences Beijing, Beijing 100083, China
3 Department of Earth Science, University of Adelaide, Adelaide, SA 5005, Australia
4 Thaines and Bodah Center for Education and Development, 203 Merinda Drive, Selah, WA 98942, USA
5 Yakima Valley College, Workforce Education & Applied Baccalaureate Programs, South 16th Avenue & Nob Hill Boulevard, Yakima, WA 98902, USA
6 Department of Civil and Environmental Engineering, Universidad de la Costa, CUC, Calle 58 # 55–66, Barranquilla 080002, Colombia
* Correspondence: alcindo.neckel@atitus.edu.br

Abstract: The use of images from the Sentinel-3B SYN satellite (surface reflectance and aerosol parameters over land) is currently one of the most advanced technologies utilized to identify atmospheric aerosol concentrations on a global scale. The general aim of this study is to analyze the evolution of aerosols in the atmosphere of the Kiev region in northern Ukraine during 2019, 2020, 2021 and 2022. Due to this study's timing, both prior to and during the current military incursion into Ukraine, this study also evaluates the consequences of the invasion of the Russian army on the territory of Ukraine, in relation to the quantitative levels of aerosols present in the atmosphere. Satellite image data were modelled in SNAP software (Sentinel Application Platform). Using the JASP software (version 0.14.1.0), clusters with variations of T550 (Aerosol Optical Thickness) were generated. The Sentinel-3B SYN satellite images were made available by the European Space Agency (ESA), with moderate spatial resolution (>300 m), calibrated and normalized to an average standard of 0.83 µg/mg, with a maximum error of 6.62% in the 30 sampled points. Satellite image data were modelled in SNAP software. Using the JASP software (version 0.14.1.0), clusters with variations of T550 (Aerosol Optical Thickness) were generated. The results show variations in the concentration of T550 in different periods, revealing that the military conflict between Russia and Ukraine directly influenced the dynamics of aerosol concentration, attributed to factors incompatible with environmental sustainability.

Keywords: remote sensing; atmospheric pollution; aerosols; geospatial analyses; global scale

Citation: Neckel, A.; Santosh, M.; Bodah, B.W.; Maculan, L.S.; Pinto, D.; Korcelski, C.; Toscan, P.C.; Cambrussi, L.P.; Caino, I.C.; Moro, L.D.; et al. Using the Sentinel-3B Satellite in Geospatial Analysis of Suspended Aerosols in the Kiev, Ukraine Region. *Sustainability* **2022**, *14*, 16357. https://doi.org/10.3390/su142416357

Academic Editor: Zihan Kan

Received: 3 November 2022
Accepted: 6 December 2022
Published: 7 December 2022

1. Introduction

Problems related to air pollution, both from natural and anthropogenic causes, are of great concern and can compromise environmental sustainability in large regions, although there are some mitigating actions for possible impacts at a global level [1–3]. Surface detailing of this information brings about greater detail [3]. Thus, the segmented images in Synthetic Aperture Radar (SAR), with deep sampling of specific super pixels allow for geospatial studies containing smooth graphical representations. Studies involving atmospheric pollution, when related to aerosol analysis, demonstrate the predominant presence of nanoparticles and fine particles, <1 µm in aerodynamic diameter, capable of remaining suspended in the atmosphere for a long period, as they possess better densities in the particulate structure [4–6]. Aerosols are nanoparticles or ultrafine particles in solid or gaseous state present in the atmosphere, originating naturally or artificially, potentiating air

contamination with concentrations of different types of chemical elements, and some are harmful to human health, capable of compromising the environmental quality of terrestrial ecosystems [7]. These atmospheric contaminants (solid particles, gases and dust), when concentrated in large amounts, are easily transported great distances, causing significant degradation to environmental quality that can affect large regions [8,9].

Previous studies analyzed [10,11] the harmful effects caused by atmospheric particulates on human health, considering aerodynamic diameters of smaller sizes of nanoparticles with 10 μm (PM_{10}) and fine particles smaller than 2.5 μm ($PM_{2.5}$). As the concentrations of atmospheric aerosols increase, the number of cases of asthma, allergies and some types of cancers linked to the respiratory system increases, compromising human health [10,11]. It has been pointed out that aerosols with high hazards to human health, in the form of nanoparticles and ultrafine particles, are mostly of metallic origin [12], such as arsenic (As), chromium (Cr), nickel (Ni), and manganese (Mn), contributing to the carcinogenic risk to the population in different age groups. It is worth considering the presence of radioactive aerosols suspended from the atmosphere, generated by nuclear installations, capable of releasing ultrafine particles of 0.01–0.1 μm in aerodynamic diameter, with a high degree of harm to human health [13]. Some pollutants, produced by chemical reactions, such as $PM_{2.5}$ and PM_{10} particles, sulphur dioxide (SO_2), nitrogen dioxide (NO_2), nobelium (NO) and ozone (O_3), are present in high amounts in the atmosphere, requiring constant measurements [14]. It should be noted that emissions of atmospheric pollutants were quantitatively reduced on a global scale due to the decrease of various industrial activities and urban mobility, starting in late 2019, and continuing throughout 2020 and 2021 due to the COVID-19 epidemic. This manuscript's satellite image analysis captured this reduction of T550 [5].

Studies have highlighted [14,15] the complexity and limitations of carrying out analyses aimed at detecting atmospheric pollutants, compromising global correlations. This is due to the need to use equipment with a high monetary cost and the difficulty of obtaining historical data, necessary for the prediction of future scenarios. The European Space Agency (ESA) subsidizes one of the most innovative solutions for detecting the concentration of aerosols present in the atmosphere on a global scale. Images captured by the Sentinel-3B satellite, combined with the use of SYN (surface reflectance and aerosol parameters over land), OLCI (Land Color Instrument) and SLSTR (Sea and Land Surface Temperature Radiometer) instrumentation, has repeatedly been shown to be one of the most modern methods in the world for the identification of aerosol levels by correction allocated to the rectangular patterns identified as T550 values (Aerosol Optical Thickness) [16–18].

Aerosols are able to become and remain suspended in the air for extended periods of time as they have low densities [4–6]. Injected into the atmosphere through soil movement/disturbance or gas release, a soil with radioactive components allows the accelerated release of dangerous elements that could be suspended in the air by wind or vehicle movements, bringing risks that could be serious to human health, even over a relatively short period of exposure [19,20].

The Kiev region of Ukraine has radioactive contaminants and other particulates present on the soil surface at relatively high levels [21]. The current and ongoing conflict between Russia and Ukraine has invoked global attention as the activities of the conflict are in regions with high levels of radiation, particularly in and around the Chernobyl evacuation zone and the currently operating Zaporizhzhia nuclear power plant [21]. Disturbances at such sites hold the potential to cause irreversible damage to environment and the health of individuals exposed to these dangerous contaminants, which can be suspended in different concentrations in the form of nanoparticles and ultrafine particles. Particles of this size are capable of remaining suspended in the air for long periods [21]. Therefore, this study, which evaluates the levels of aerosols present in the atmosphere in the Kiev region both prior to and during the current, ongoing conflict, is highly significant. Furthermore, this study also highlights the importance of using the Sentinel-3B SYN satellite in a current

conflict zone where the entry of civilians is prohibited, enabling the detection of aerosol levels in what may be otherwise inaccessible territorial regions [4–6].

In view of the problem faced by the difficulty of analyzing gaseous contaminants, it is necessary to follow up through new technologies, such as remote sensing, which provides images of various sensors and resolutions for free, helping to monitor changes that occur in or around it. Given this backdrop, the general aim of this study is to analyze the evolution of aerosols in the atmosphere of the Kiev region of Ukraine, in periods sampled in the years 2019, 2020, 2021 and 2022. In addition to evaluating the consequences of the advancement of the Russian army into Ukrainian territory, in relation to the quantitative levels of aerosols present in the atmosphere.

This study stands out for its use of one of the most modern techniques in the world for detecting the levels of atmospheric aerosols in and around Kiev, the capital of Ukraine. The authors intent is to stimulate a global discussion through the use of unprecedented images from the Sentinel-3B SYN satellite over the course of 2022. This makes this study a benchmark for other researchers, regarding the concerns that can generate unsustainability through elevated levels of temporary T550 exposure to all those residing in and around Kiev.

2. Materials and Methods

2.1. Study Area

The capital city of Kiev is located in northern Ukraine and has a total land area of 839 km^2 (Figure 1 (maps in UTM coordinates—Universal Transverse Mercator)). Kiev's 2021 population was 2,962,180 inhabitants [22]. The predominant climate in Ukraine is defined as continental temperate, with hotter summers in the south and east, and colder winters in the east and north of the country. The region's highest annual temperatures occur in July, with an average high of 26.28 °C. The lowest annual temperatures occur in January, with an average low of −6.07 °C [23]. The wettest month of the year is June which records an annual average of 71.55 mm of precipitation, while February has the lowest annual average of 35.34 mm of precipitation [23,24].

2.2. Details Regarding the Ongoing Military Conflict between Russia and Ukraine

On 24 February 2022, an internationally recognized illegal incursion into Ukrainian territory began as Russian forces invaded the country. This continues to have wide ranging impacts on social, economic, cultural and environmental sectors not only in Ukraine but world-wide [25]. This illegal action has compromised Russia's world standing in addition to its ties and investments with the West. This has resulted in direct impacts around access to goods and essential components for the natural gas and insecticide industries, consequently affecting the global economy and inflating the price of many important products that are essential for the world's population [21,25]. In this study, we analyze the evolution of aerosols in the atmosphere in the city of Kiev over the period from 2019 to 2022. Data from the year 2022 focuses on before and after the Russian invasion in Ukraine.

2.3. Satellite Data Pre-Processing

Satellite images used for this study were captured on 20 September 2019; 18 August 2020; 15 August 2021; 19 March 2022; 23 March 2022 15 April 2022 and 2 July 2022. The images used in the year 2022 consist of unpublished images made available by ESA through the researcher's login access and did not continue after the date of 2 July 2022 due to lack of availability from ESA. The increase in sampling dates in 2022 was due to the continually evolving situation of the military conflict in Ukraine. The geospatial collection dates were selected from the visual quality of the Sentinel-3B SYN satellite images, determined by the absence of cloud shadow over the study area [16].

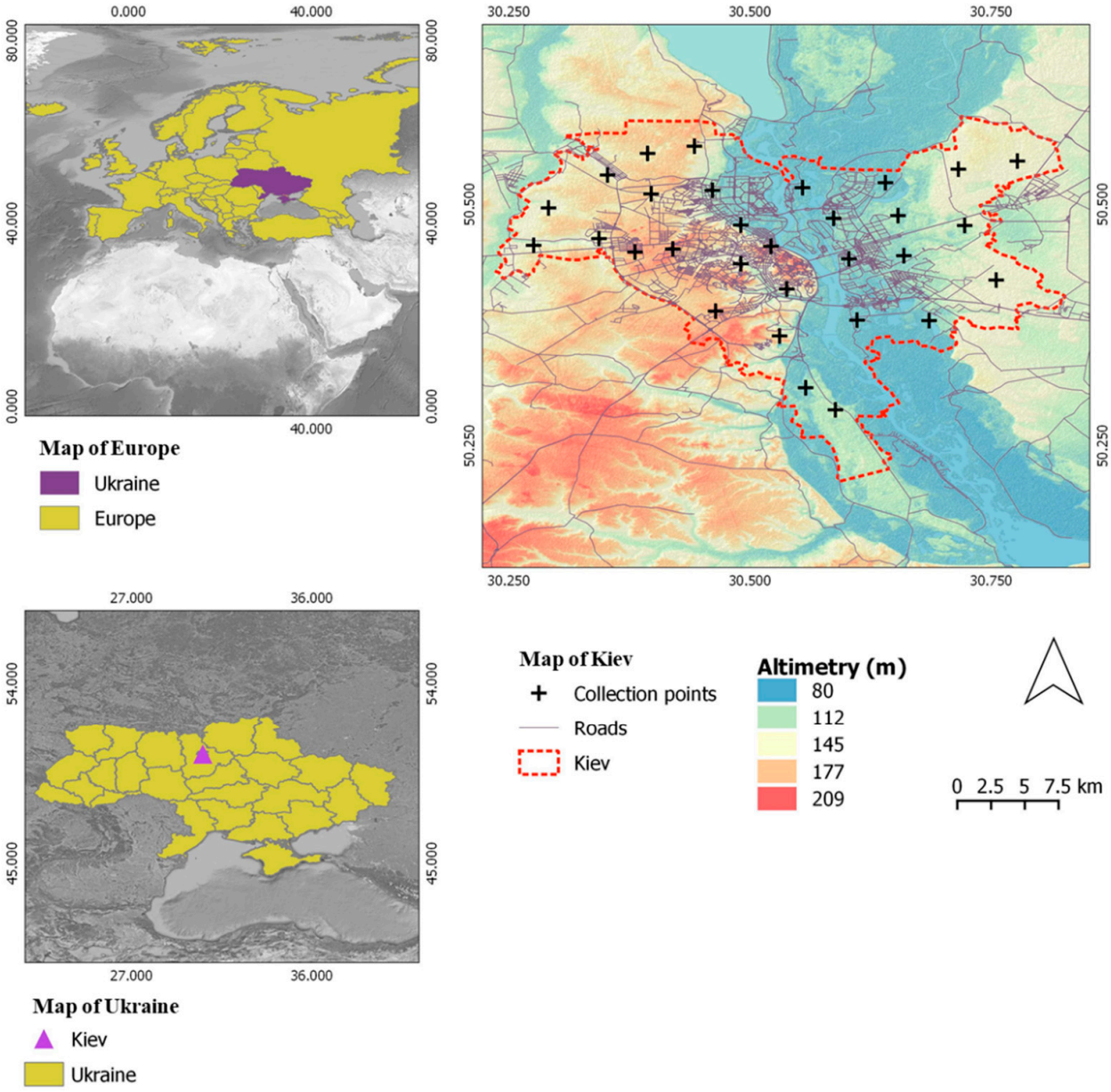

Figure 1. Location of Kiev, the capital city of Ukraine, and the grid of data collection points used for aerosol analysis. Source: Adapted from the map-graphic database of Kiev [24].

The Sentinel-3B SYN satellite images were captured through the ONDA Catalog, made available by ESA linked to the Copernicus Program [18]. These images were processed by the Sentinel-3B SYN, provided by an Earth Satellite Observation (EO) mission, designed in the operational service of ESA's Global Land and Ocean Mission (GMES) [18]. In addition, the images used in this study have optical data of repeated global coverage of 1–2 days with moderate spatial resolution (>300 m), using the SLSTR (Payload Sea and Land Surface Temperature Radiometer) and OLCI (Ocean and Land Color Instrument), which provide accurate information, along with greater detail of the Earth's surface [26,27]. Thus, the Sentinel-3B SYN satellite images were calibrated and classified by the ESA, with normalization with the average standard of 0.83 µg/mg, with a maximum error of 6.62%, ensuring that the hyperparameters can remain unchanged during the collection experiment in each of the 30 sampled points [18], creating a methodological standard on an online platform for researchers who have access to the ESA login.

The criterion for choosing the positioning of the 30 sampled points was based on representation by the Triangulated Irregular Network (TIN) in spacing between points, available in the scientific literature, of 1 to 3 km [28–30]. The Level-2 SYN (SY_2_SYN) product uses the Earth's surface reflectance and the parameters of the geophysical structures of aerosols, for the definition of Aerosol Optical Thickness (AOT), collected from a sine wave, with a geospatial length of 550 nm (T550) [18], generating maximum and minimum reflectance values, capable of representing the thickness of the T550 at each of the points collected in the Sentinel-3B SYN satellite images. The wavelength consists of the distance, where certain values have a wave pattern, differentiating themselves through the heterogeneity of the physical structures that form the elements, captured by the infrared sectors of the satellites [31–34].

The Sentinel-3B SYN satellite images were processed using SNAP software (Sentinel Application Platform), volume 8.0., based on the applied technology of components and controls of Geographic Information Systems (GIS). This yields a corresponding measurement of T550 at different altitudes (Alt), specific to data collection (aerosol levels), captured from the structure of nanoparticles and ultrafine particles by wavelength [18], and based on the 30 points determined by the TIN network. This set of methodological data were used in this study because it is one of the most modern techniques for identifying aerosol levels world-wide [5].

Data on aerosol levels collected at the 30 points by images from the Sentinel-3B SYN satellite in the city of Kiev formed a single database. Subsequently, they were modeled statistically in k-means clusters, using JASP software (version 0.14.1.0), in which it was possible to understand the data vector algorithms, optimized by clusters forming clusters [35,36]. Consequently, the generated clusters yielded the Silhouette index, based on the consistency of the internal average of the evaluated clusters, through the degree of similarity of each cluster [35–37].

Silhouette scores indicate that the closer the value is to 1, the more reliability and consistency the sample data have, and the value of −1 can be related to an imprecision of the data [35,38,39]. Cluster analysis [35–39] facilitates a better understanding of the results acquired through collected data, facilitating the understanding of aerosol dispersion in the city of Kiev through Sentinel-3B SYN satellite images. Clusters were plotted on a Gaussian kernel density plot, smoothed from canopy height distributions (>0 m) based on a stratified random sample from each cluster [35,36]. Each of the clusters is assigned a specific color, with a detailed legend of the clusters' color assignments in each variable, in addition to the overlaps present in the variables [35,36,39].

3. Results and Discussion

The results of this study showed that T550 averages were detected at higher concentrations in the sampled period of 2020 (August 18th) and 2021 (August 15th) (Table 1). The maximum value of T550 occurred in 2020 (0.894 nm) and the lowest minimum value occurred in 2022. In this way, it is possible to determine that there was a reduction for T550 in the periods sampled in 2022, when compared to the period analyzed in 2019, 2020 and 2021 (Table 1). Again, it must be remembered that the world experienced a significant decrease in industrial activities and the use of motor vehicles during the global COVID-19 pandemic, which was reflected in the data sets obtained [5] and may have also lowered overall air pollutants in Ukraine in 2019, 2020 and 2021. This may well have impacted the results of this study, in relation to the levels of pre-conflict T550 that were collected in the satellite imagery utilized. Despite the great concern of the international community regarding the consequences of aerosol dispersion by the Russian invasion of Ukrainian territory.

Table 1. Descriptive statistics of the data collected at the 30 points sampled from the Sentinel-3B SYN satellite images in the city of Kiev, Ukraine.

Items	Geospatial Image Collection Period from the Sentinel-3B SYN Satellite						
	2019-09-30	**2020-08-18**	**2021-08-15**	**2022-03-19**	**2022-03-23**	**2022-04-15**	**2022-07-02**
Valid	30	30	30	30	30	30	30
Missing value	0	0	0	0	0	0	0
Average	0.513 (nm)	0.592 (nm)	0.380 (nm)	0.290 (nm)	0.370 (nm)	0.356 (nm)	0.354 (nm)
Standard deviation	0.091 (nm)	0.158 (nm)	0.106 (nm)	0.094 (nm)	0.111 (nm)	0.081 (nm)	0.125 (nm)
Minimum	0.387 (nm)	0.305 (nm)	0.239 (nm)	0.160 (nm)	0.185 (nm)	0.232 (nm)	0.187 (nm)
Maximum	0.667 (nm)	0.894 (nm)	0.575 (nm)	0.492 (nm)	0.694 (nm)	0.518 (nm)	0.578 (nm)

Prior to 24 February 2022, rather low aerosol levels were detected over Kiev utilizing Sentinel-3B SYN satellite. This can be attributed to the low occurrence of soil movement in the stable Kiev region along with the influence of decreasing industrial activities due to the global pandemic [21]. This area's soils contain radioactive substances present on the soil surface. The T550 values published in this study do not show an increase over the period of analysis.

When related to the Russian invasion of Ukraine, we need to consider the factors detected in previous research that contribute to the lack of sustainability in military conflicts. We highlight the following features: negative commitment to the world economy, impacts on geopolitics and food security that compromise local sustainability and energy reserves [21,40]; environmental crimes [41]; scarcity of monetary resources at the local level, the capability of further compromising the livelihood of low-income families [42]; possible bankruptcy of large, medium and small companies [43]; impacts on diesel distribution, compromising sustainable clean energy markets in Europe, trade in platinum, gold, palladium and nickel, among other metals [44]; and decreased consumption of Russian commodities, attributed to 73 countries, which can impact markets to differing degrees, resulting from the import and export of products [45]. In addition to the commitment to the distribution of gas in Europe, regressing in terms of environmental sustainability, the resumption of the use of mineral coal for the production of energy increase the levels of atmospheric pollution, harmfully compromising the quality of human health [46].

High levels of air pollution can cause problems to human health, such as cancers attributed to the respiratory system, in addition to allergies, asthma, among other diseases related to the presence of metallic or radioactive contaminants, in physical structures, in the form of nanoparticles and ultrafine particles suspended in the air for a long period, as they have less density in relation to other elements [5,47–50]. The existence of aerosols in the atmosphere must be taken into account, in the sense of admitting their harmfulness to human health [5,49,50]. In this perspective, the average results of T550 (Table 2) did not demonstrate high levels of aerosols in the sampled collection period in the Kiev region. A probable hypothesis may be linked to the reduction of atmospheric gases due to the lessing or overall stoppage of industrial activities due to the COVID-19 pandemic, along with the reduction in the use of motor vehicles, which could explain the lower levels of aerosols [5]. However, the existence of these aerosols in the atmosphere cannot be excluded, and their levels may increase, with the possibility of movement of particles presently confined in the soil due to activities related to the military incursion.

Table 2. Representation of clusters originated from data collected at 30 points sampled from the Sentinel-3B SYN satellite images in the city of Kiev, Ukraine.

Cluster	1	2	3
Size	12	10	8
Explained proportion within-cluster heterogeneity	0.448	0.324	0.228
Within sum of squares	44.601	32.263	22.721
Silhouette score	0.274	0.315	0.321

Regarding the K-means analysis, the adjustment scores for the model are presented, in which k = 3 clusters, considering a data set of 30 collection points, with an R^2 value of 0.509. Data from the Akaike Information Criterion (AIC) and Bayesian Information Criterion (BIC) models were tested, which, despite measuring the model's goodness of fit, penalize the number of free parameters, and the models that have criteria of information, when compared to the model used in the JASP software [51]. The data, when subjected to statistical tests, allow greater reliability in relation to the demonstration of the results in the research [51–53].

In this study, the Silhouette index ranged from zero (0) to one (1), with the representativeness of k = 3 clusters and 0.3 in the clustering trend, according to the variables established [35–37]. Table 2 shows the cluster sizes, the variability within each cluster in terms of the sum of squares, the proportion of explained heterogeneity within the cluster and the Silhouette index. As for heterogeneity, the total value 1 is proportionally divided. Cluster 1 is the largest with 12 collection points and heterogeneity of 0.448, demonstrating greater heterogeneity between clusters. Meanwhile, Cluster 3 is the most homogeneous, with 8 points and a proportion of 0.228, showing high heterogeneity. Cluster 2 presented 10 collection points and heterogeneity of 0.324 (Table 2). Another parameter capable of evaluating a cluster is the sum of squares, that is, the lower the sum of squares, the lower the variability [36,37]. Cluster 3 has the lowest sum of squares with 29,344, that is, the most homogeneous; while Cluster 1 is the most heterogeneous with 44,601.

The Silhouette index shows greater homogeneity and cohesion, where the best results were identified in Cluster 3, with an index of 0.321. Cluster 1 shows an index of 0.274 and Cluster 2 of 0.315. These values demonstrate that there is reasonable homogeneity within each cluster, as well as demonstrating that the differences between Clusters 1 and 3 are significant and that Cluster 2 signals an intermediate cluster.

When considering the range for each variable (clusters means), the midpoint and the scope of each cluster, represented by Gaussian kernel density graphs, smoothed in canopy height (>0 m), are stratified randomly in each cluster [38,39]. In this context, our results highlight a greater overlap of the densities of Cluster 2 over Clusters 1 and 3, when checking the intermediate characteristics of the clusters (Figure 2).

In relation to Figure 2, these T550 (nm) concentration differences are reduced in the analyzed periods of 2022 (Figure 2D–G). When relating to other studies that investigated the levels of atmospheric pollution [3,54–59], it is pointed out that the high levels with concentrations of atmospheric aerosols related to the release of pollutants by industrial production activities. In this relationship, the decrease in aerosol concretion in the Kiev region (Figure 2D–G) can be attributed to the stoppage of most industrial activities, after 24 February 2022, when the conflict between Russia and Ukraine began.

The general analysis of the clusters demonstrates a centralization of the highest concentrations of aerosols (Cluster 1) in the city of Kiev (Figure 3); while intermediate values (Cluster 2) and lower values (Cluster 3) were located on the periphery (Figure 3). These data indicate a greater concentration of aerosols in the center of the city, in areas of greater urbanization, with a greater incidence of bombing activities resulting from the military conflict, where many cars and people are located, in addition to a greater concentration of industry, despite most being limited due to the pandemic [21].

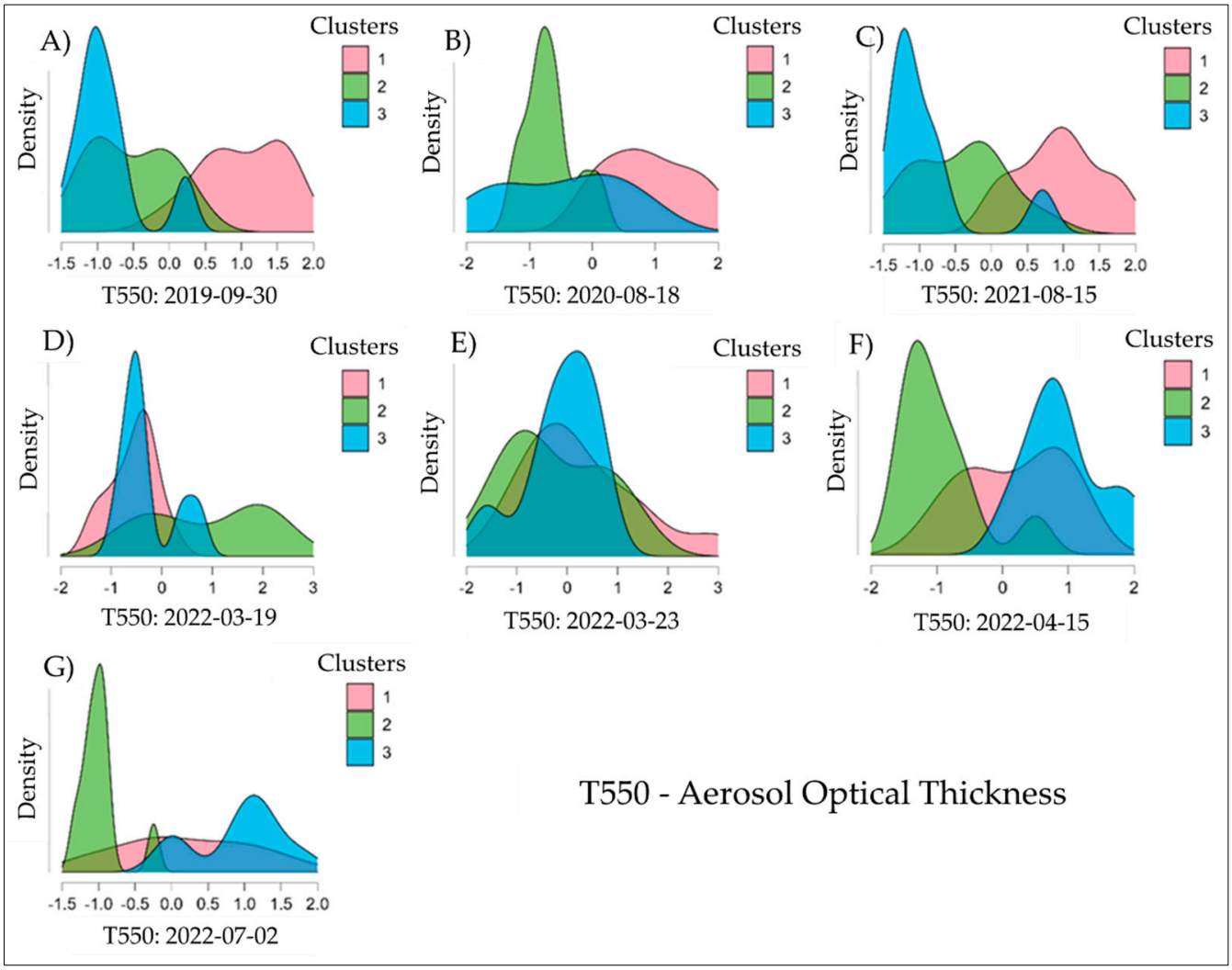

Figure 2. Representation of the results of the collection period in graphs of Gaussian kernel year density, stratified randomly in each cluster, from the following period: (**A**) T550: 2019-09-30; (**B**) T550: 2020-08-18; (**C**) T550: 2021-08-15; (**D**) T550: 2022-03-19; (**E**) T550: 2022-03-23; (**F**) T550: 2022-04-15; (**G**) T550: 2022-07-02.

Based on the 30 points in Kiev for which Sentinel-3B SYN satellite images were analyzed (Figure 4), we note a decline in aerosol concentrations between the periods of 2019, 2020, 2021, in which the highest concentrations of aerosols occurred in downtown Kiev (Figure 4A–C) during the 2022 analysis (Figure 4D–G). At this time, the location of the highest concentrations of aerosols moved from the center of Kiev (T550 = 0.274 nm) to the periphery (T550: 19 March 2022; Figure 4D) where T550 values ranged from 0.315 nm to 0.321 nm. This may be related to the initial conflicts in the border region between Ukraine and Russia. The impacts of military action in relation to the projection of high levels of aerosols are confirmed at the border (T550 = 0.321 nm) and in the center of the city of Kiev (T550 = 0.274 nm), during the period of advance of Russian troops (Figure 4B), demonstrating greater atmospheric contamination by aerosols.

Figure 4E–G shows the significant differences with item C (T550: 15 August 2021), a time when Russian troops were not yet present in Ukraine and the country (especially Kiev) was not being targeted by Russian artillery strikes. Thus, it can be confirmed that the invasion of Russian troops caused the significant increase and variations in aerosol concentrations in the city of Kiev. Even with the decrease in aerosol concentrations due to the stoppage of industrial activities due to these bombing raids, the accumulation of

atmospheric aerosols can be seen due to the movement of troops, which can be even more worrying, since the soil of the Kiev region potentiates a high load of hazardous elements, such as: iron, zinc, nickel, arsenic, cadmium, lead, aluminum, mercury, titanium, tungsten, tin, cobalt, and chromium, in addition to the high load of radioactive elements, historically aggravated by the Chernobyl accident, which left high levels of radionuclides in the soil [21,60–63].

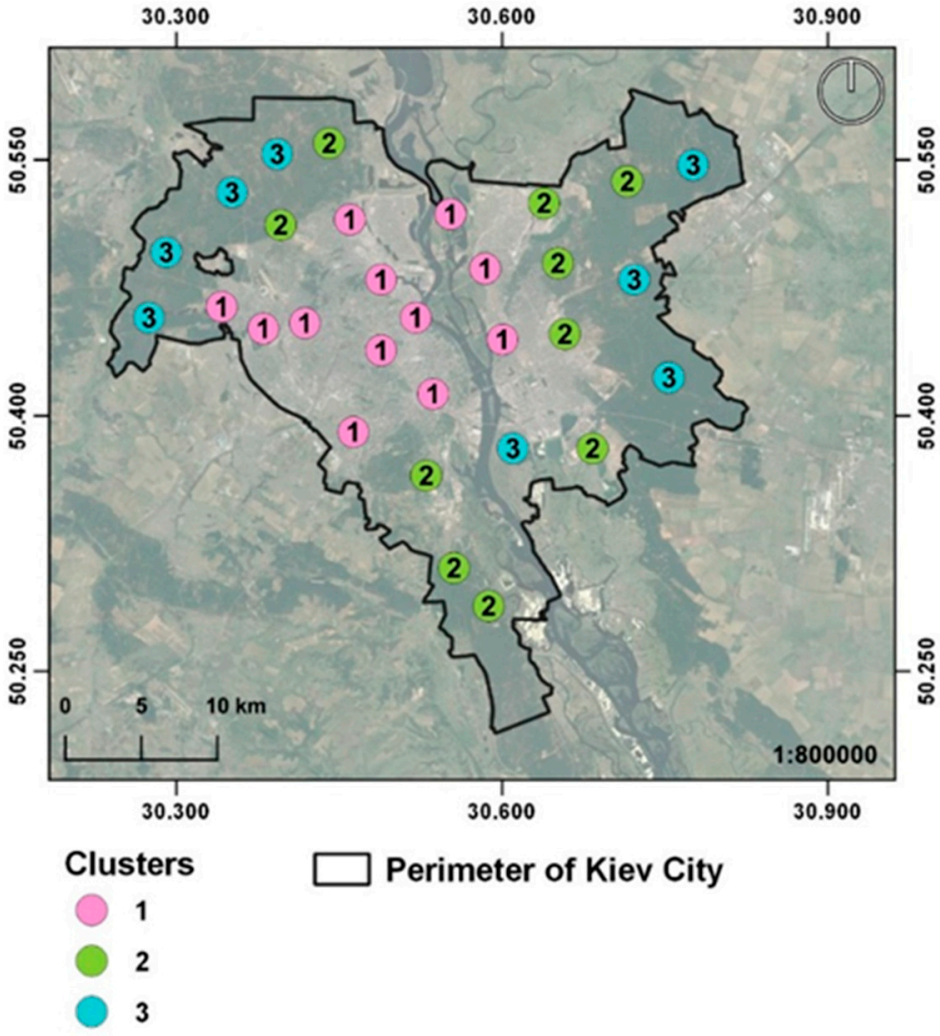

Figure 3. Cluster of clusters identified from Sentinel-3B SYN satellite images in the city of Kiev, Ukraine. Source: Based on the ESA database.

In addition, Figure 4 represents the aerosol concentration dynamics collected at the 30 points sampled by Sentinel-3B SYN satellite images in the city of Kiev, demonstrating that the average of 0.513 (T550: 30 September 2019) for high concentrations of T550, and those that have proportions in low averages of 0.354 (T550: 2 July 2022) (Table 1). These concentrations are of great concern, as they the levels of aerosol concentration are considered high when compared to other studies carried out utilizing satellite images globally in which the negative effects of air pollution on human health were identified, particularly with the increase in respiratory and cancer diseases. In addition to the concentrations of T550, when related to the average degree of optical thickness, these studies showed average variations from 0.200 to 0.907 [5,64–66]. This situation reinforces the importance of this study, focused on the city of Kiev, where military conflict can inject even more nanoparticles and ultrafine particles into the atmosphere, which can cause irreversible damage to the health of the population.

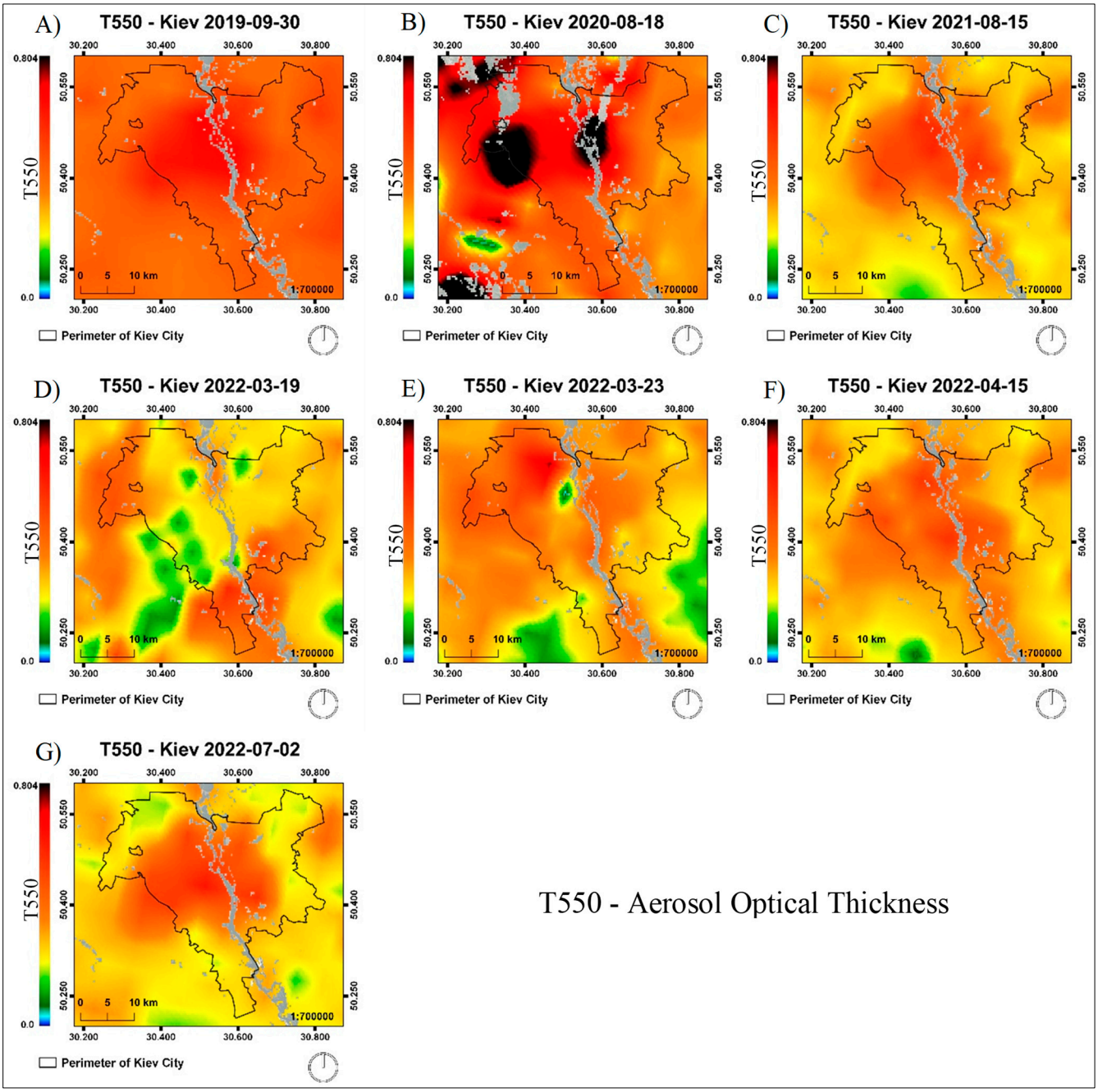

Figure 4. Identification of aerosol levels collected in Sentinel-3B SYN satellite images in the city of Kiev (Ukraine), from the following periods: (**A**) T550: 30 September 2019; (**B**) T550: 18 August 2020; (**C**) T550: 15 August 2021; (**D**) T550: 19 March 2022; (**E**) T550: 23 March 2022; (**F**) T550: 15 April 2022; (**G**) T550: 2 July 2022. Source: Based on the ESA database.

4. Conclusions

The variations in airborne concentration of T550 through the use of images from the Sentinel-3B SYN satellite collected over 2019, 2020, 2021 and 2022 spoke to the dynamics present over Kiev during this time frame. The authors suggest future application of the Fast Task-Specific Region Merging for SAR Image Segmentation methods; Fast SAR Image Segmentation with Deep Task-Specific Super pixel Sampling; and Soft Graph Convolution for a better understanding of the geospatial dynamics of the terrestrial environment of the city of Kiev. Consequently, it becomes important to highlight the need to reflect the high

generalization capacity of the dynamics of atmospheric aerosols over Kiev, emphasizing the need for the continuity of others to carry out more studies on these T550 variations.

The beginning of the Russian military incursion into Ukraine led to an increase in the concentrations of T550 in the regions around the city of Kiev. As the conflict intensified, these concentrations rose toward the center of the Kiev proper. The analysis of aerosols through satellites helped to emphasize recent studies aimed at understanding situations in this area of conflict, which may compromise global sustainability. In this context, future studies are recommended, particularly to continue the assessment of T550 levels in the Kiev region, with the realization and testing of other statistical methods aimed at modelling future quantitative data. Such an attempt would assist in the identification of certain concentrations of aerosols from a geospatial perspective, which can lessen environmental sustainability overall.

Author Contributions: Conceptualization, L.D.M., I.C.C. and D.P.; data curation, L.S.M.; formal analysis, A.N. and C.C.O.d.A.S.; funding acquisition, B.W.B., D.P.J. and A.N.; investigation, L.D.M.; project administration, C.K. and D.P.; supervision, P.C.T. and L.P.C.; visualization, A.N. and L.P.C.; writing—original draft preparation, A.N. and M.S.; writing—review and editing, G.d.V.M., G.T.C. and M.S. All authors have read and agreed to the published version of the manuscript.

Funding: This research received no external funding.

Institutional Review Board Statement: Not applicable.

Informed Consent Statement: Informed consent was obtained from all subjects involved in the study.

Data Availability Statement: Not applicable.

Acknowledgments: The authors are grateful to the European Space Agency (ESA) and the U.S. National Aeronautics and Space Administration (NASA) for providing the unpublished and treated Sentinel-3B satellite images. We also wish to thank the Center for Studies and Research on Urban Mobility (NEPMOUR+S/ATITUS), Fundação Meridional, Brazil and the Brazilian National Council for Scientific and Technological Development (CNPq).

Conflicts of Interest: The authors declare no conflict of interest.

References

1. Mao, S.; Lang, J.; Chen, T.; Cheng, S. Improving source inversion performance of airborne pollutant emissions by modifying atmospheric dispersion scheme through sensitivity analysis combined with optimization model. *Environ. Pollut.* **2021**, *284*, 117186. [CrossRef] [PubMed]
2. Leng, S.; Li, S.W.; Hu, Z.Z.; Wu, H.Y.; Li, B.B. Development of a micro-in-meso-scale framework for simulating pollutant dispersion and wind environment in building groups. *J. Clean. Prod.* **2022**, *364*, 132661. [CrossRef]
3. Zhang, X.; Wang, J. Atmospheric dispersion of chemical, biological, and radiological hazardous pollutants: Informing risk assessment for public safety. *JSSR* **2022**, *3*, 372–397. [CrossRef]
4. Félix, O.I.; Csavina, J.; Field, J.; Rine, K.P.; Sáez, A.E.; Betterton, E.A. Use of lead isotopes to identify sources of metal and metalloid contaminants in atmospheric aerosol from mining operations. *Chemosphere* **2015**, *122*, 219–226. [CrossRef]
5. Bodah, B.W.; Neckel, A.; Stolfo Maculan, L.; Milanes, C.B.; Korcelski, C.; Ramírez, O.; Mendez-Espinosa, J.F.; Bodah, E.T.; Oliveira, M.L. Sentinel-5P TROPOMI satellite application for NO_2 and CO studies aiming at environmental valuation. *J. Clean. Prod.* **2022**, *357*, 131960. [CrossRef]
6. Jiao, X.; Zeng, R.; Lan, G.; Zuo, S.; He, J.; Wang, C. Mechanistic study on photochemical generation of I●/I2●− radicals in coastal atmospheric aqueous aerosol. *Sci. Total Environ.* **2022**, *825*, 154080. [CrossRef]
7. Wang, H.; He, C.; Modini, R.L.; Wang, W.; Lu, H.; Morawska, L. Mixing state of printer generated ultrafine particles: Implications for the complexity of indoor aerosols. *Atmos. Environ.* **2021**, *259*, 118550. [CrossRef]
8. Chen, S.; Zhang, R.; Mao, R.; Zhang, Y.; Chen, Y.; Ji, Z.; Gong, Y.; Guan, Y. Sources, characteristics and climate impact of light-absorbing aerosols over the Tibetan Plateau. *Earth-Sci. Rev.* **2022**, *232*, 104111. [CrossRef]
9. Yang, J.; Zhao, C.; Sun, Y.; Chi, Y.; Yang, Y. Aerosol first indirect effect over narrow longitude regions of North Pacific and same-latitude lands. *Atmos. Environ.* **2022**, *277*, 119081. [CrossRef]
10. Li, N.; Georas, S.; Alexis, N.; Fritz, P.; Xia, T.; Williams, M.A.; Horner, E.; Nel, A. A work group report on ultrafine particles (American Academy of Allergy, Asthma & Immunology): Why ambient ultrafine and engineered nanoparticles should receive special attention for possible adverse health outcomes in human subjects. *J. Allergy Clin. Immunol.* **2016**, *138*, 386–396. [CrossRef]

11. Moreno-Ríos, A.L.; Tejeda-Benítez, L.P.; Bustillo-Lecompte, C.F. Sources, characteristics, toxicity, and control of ultrafine particles: An overview. *Geosci. Front.* **2020**, *13*, 101147. [CrossRef]
12. Fan, M.Y.; Zhang, Y.L.; Lin, Y.C.; Cao, F.; Sun, Y.; Qiu, Y.; Xing, G.; Dao, X.; Fu, P. Specific sources of health risks induced by metallic elements in $PM_{2.5}$ during the wintertime in Beijing, China. *Atmos. Environ.* **2021**, *246*, 118112. [CrossRef]
13. Lee, M.H.; Yang, W.; Chae, N.; Choi, S. High resolution size characterization of particulate contaminants for radioactive metal waste treatment. *Nucl. Eng. Technol.* **2021**, *53*, 2277–2288. [CrossRef]
14. Middya, A.I.; Roy, S. Pollutant specific optimal deep learning and statistical model building for air quality forecasting. *Environ. Pollut.* **2020**, *301*, 118–972. [CrossRef]
15. Mohammadshirazi, A.; Kalkhorani, V.A.; Humes, J.; Speno, B.; Rike, J.; Ramnath, R.; Clark, J.D. Predicting airborne pollutant concentrations and events in a commercial building using low-cost pollutant sensors and machine learning: A case study. *Build. Environ.* **2022**, *213*, 108833. [CrossRef]
16. Fernandez-Moran, R.; Gómez-Chova, L.; Alonso, L.; Mateo-García, G.; López-Puigdollers, D. Towards a novel approach for Sentinel-3 synergistic OLCI/SLSTR cloud and cloud shadow detection based on stereo cloud-top height estimation. *ISPRS J. Photogramm. Remote Sens.* **2021**, *181*, 238–253. [CrossRef]
17. Neckel, A.; Oliveira, M.L.; Castro Bolaño, L.J.; Maculan, L.S.; Moro, L.D.; Bodah, E.T.; Moreno-Ríos, A.L.; Bodah, B.W.; Silva, L.F. Biophysical matter in a marine estuary identified by the Sentinel-3B OLCI satellite and the presence of terrestrial iron (Fe) nanoparticles. *Mar. Pollut. Bull.* **2021**, *173*, 112925. [CrossRef]
18. ESA. European Space Agency. Sentinel-5P Pre-Operations Data Hub–European, 2022. Available online: https://s5phub.copernicus.eu/dhus/ (accessed on 1 August 2022).
19. Sanusi, M.; Ramli, A.; Hassan, W.; Lee, M.; Izham, A.; Said, M.; Wagiran, H.; Heryanshah, A. Assessment of impact of urbanisation on background radiation exposure and human health risk estimation in Kuala Lumpur, Malaysia. *Environ. Int.* **2017**, *104*, 91–101. [CrossRef]
20. Xu, C.; Zhang, Z.; Ling, G.; Wang, G.; Wang, M. Air pollutant spatiotemporal evolution characteristics and effects on human health in North China. *Chemosphere* **2022**, *294*, 133814. [CrossRef]
21. Pereira, P.; Bašić, F.; Bogunovic, I.; Barcelo, D. Russian-Ukrainian war impacts the total environment. *Sci. Total Environ.* **2022**, *837*, 155865. [CrossRef]
22. UKRCENSUS. State Statistics Service of Ukraine. All-Ukrainian Population Censos, 2021. Available online: https://www.ukrcensus.gov.ua/eng/ (accessed on 10 August 2022).
23. Climate Change Knowledge Portal. Ukraine, 2022. Available online: https://climateknowledgeportal.worldbank.org/country/ukraine/climate-data-historical (accessed on 10 August 2022).
24. Simplemaps. Ukraine Cities Database, 2022. Available online: https://simplemaps.com/data/ua-cities (accessed on 18 August 2022).
25. Racioppi, F.; Rutter, H.; Nitzan, D.; Borojevic, A.; Carr, Z.; Grygaski, T.J.; Jarosińska, D.; Netanyahu, S.; Schmoll, O.; Stuetzle, K.; et al. The impact of war on the environment and health: Implications for readiness, response, and recovery in Ukraine. *Lancet* **2022**, *400*, 871–873. [CrossRef]
26. Fletcher, K. *Sentinel-2: ESA's Optical High-Resolution Mission for GMES Operational Services*; ESA Communications: Oakville, ON, Canada, 2012; ISBN 978-92-9221-419-7.
27. Moro, L.D.; Maculan, L.S.; Pivoto, D.; Cardoso, G.T.; Pinto, D.; Adelodun, B.; Bodah, B.W.; Santosh, M.; Bortoluzzi, M.G.; Branco, E.; et al. Geospatial Analysis with Landsat Series and Sentinel-3B OLCI Satellites to Assess Changes in Land Use and Water Quality over Time in Brazil. *Sustainability* **2022**, *14*, 9733. [CrossRef]
28. Clevis, Q.; Tucker, G.E.; Lancaster, S.T.; Desitter, A.; Gasparini, N.; Lock, G. A simple algorithm for the mapping of TIN data onto a static grid: Applied to the stratigraphic simulation of river meander deposits. *Comput. Geosci.* **2006**, *32*, 749–766. [CrossRef]
29. Refice, A.; Giachetta, E.; Capolongo, D. SIGNUM: A Matlab, TIN-based landscape evolution model. *Comput. Geosci.* **2012**, *45*, 293–303. [CrossRef]
30. Goellner, E.; Neckel, A.; Bodah, B.W.; Maculan, L.S.; Almeida Silva, C.C.O.D.; Piccinato, D.; Grub, J.; Cambrussi, L.P.; Korcelski, C.; Oliveira, M.L. Geospatial analysis of Ae. aegypti foci in southern Brazil. *J. Environ. Chem. Eng.* **2021**, *9*, 106645. [CrossRef]
31. Ialongo, I.; Stepanova, N.; Hakkarainen, J.; Virta, H.; Gritsenko, D. Satellite-based estimates of nitrogen oxide and methane emissions from gas flaring and oil production activities in Sakha Republic, Russia. *Atmos. Environ. X.* **2021**, *11*, 100114. [CrossRef]
32. Sarkar, T.; Anand, S.; Bhattacharya, A.; Sharma, A.; Venkataraman, C.; Sharma, A.; Ganguly, D.; Bhawar, R. Evaluation of the simulated aerosol optical properties over India: COALESCE model inter-comparison of three GCMs with ground and satellite observations. *Sci. Total Environ.* **2022**, *852*, 158442. [CrossRef]
33. Trujillo-Acatitla, R.; Tuxpan-Vargas, J.; Ovando-Vázquez, C. Oil spills: Detection and concentration estimation in satellite imagery, a machine learning approach. *Mar. Pollut. Bull.* **2022**, *184*, 114132. [CrossRef]
34. Alandihallaj, M.A.; Emami, M.R. Satellite replacement and task reallocation for multiple-payload fractionated Earth observation mission. *Acta Astronaut.* **2022**, *196*, 157–175. [CrossRef]
35. Naghizadeh, A.; Metaxas, D.N. Condensed Silhouette: An Optimized Filtering Process for Cluster Selection in K-Means. *Procedia Comput. Sci.* **2020**, *176*, 205–214. [CrossRef]
36. Maroni, D.; Cardoso, G.T.; Neckel, A.; Maculan, L.S.; Oliveira, M.L.; Bodah, E.T.; Bodah, B.W.; Santosh, M. Land surface temperature and vegetation index as a proxy to microclimate. *J. Environ. Chem. Eng.* **2021**, *9*, 105796. [CrossRef]

37. Niu, G.; Ji, Y.; Zhang, Z.; Wang, W.; Chen, J.; Yu, P. Clustering analysis of typical scenarios of island power supply system by using cohesive hierarchical clustering based K-Means clustering method. *Energy Rep.* **2021**, *7*, 250–256. [CrossRef]
38. Borlea, I.D.; Precup, R.E.; Borlea, A.B. Improvement of K-means Cluster Quality by Post Processing Resulted Clusters. *Procedia Comput. Sci.* **2022**, *199*, 63–70. [CrossRef]
39. Ahmad, A.; Khan, S.S. initKmix-A novel initial partition generation algorithm for clustering mixed data using k-means-based clustering. *Expert Syst. Appl.* **2021**, *167*, 114149. [CrossRef]
40. Zhou, X.Y.; Lu, G.; Xu, Z.; Yan, X.; Khu, S.T.; Yang, J.; Zhao, J. Influence of Russia-Ukraine War on the Global Energy and Food Security. *Resour. Conserv. Recycl.* **2023**, *188*, 106657. [CrossRef]
41. Rawtani, D.; Gupta, G.; Khatri, N.; Rao, P.K.; Hussain, C.M. Environmental damages due to war in Ukraine: A perspective. *Sci. Total Environ.* **2022**, *850*, 157932. [CrossRef]
42. Khalfaoui, R.; Gozgor, G.; Goodell, J.W. Impact of Russia-Ukraine war attention on cryptocurrency: Evidence from quantile dependence analysis. *Financ. Res. Lett.* **2022**, *49*, 103365. [CrossRef]
43. Bougias, A.; Episcopos, A.; Leledakis, G.N. Valuation of European firms during the Russia–Ukraine war. *Econ. Lett.* **2022**, *218*, 110750. [CrossRef]
44. Umar, M.; Riaz, Y.; Yousaf, I. Impact of Russian-Ukraine war on clean energy, conventional energy, and metal markets: Evidence from event study approach. *Resour. Policy* **2022**, *79*, 102966. [CrossRef]
45. Lo, G.D.; Marcelin, I.; Bassène, T.; Sène, B. The Russo-Ukrainian war and financial markets: The role of dependence on Russian commodities. *Financ. Res. Lett.* **2022**, *50*, 103194. [CrossRef]
46. Adekoya, O.B.; Oliyide, J.A.; Yaya, O.S.; Al-Faryan, M.A.S. Does oil connect differently with prominent assets during war? Analysis of intra-day data during the Russia-Ukraine saga. *Resour. Policy* **2022**, *77*, 102728. [CrossRef]
47. Silva, L.F.; Oliveira, M.L.; Milanes, C.B.; Bodah, B.W.; Cambrussi, L.P.; Dotto, G. Effects of atmospheric pollutants on human health and deterioration of medieval historical architecture (North Africa, Tunisia). *Urban Clim.* **2022**, *41*, 101046. [CrossRef]
48. Silva, L.F.O.; Pinto, D.; Neckel, A.; Oliveira, M.L.S.; Sampaio, C.H. Atmospheric nanocompounds on Lanzarote Island: Vehicular exhaust and igneous geologic formation interactions. *Chemosphere* **2020**, *254*, 1–14. [CrossRef]
49. Oliveira, M.L.; Pinto, D.; Zanchett, M.R.D.; Silva, L.F. Air pollutants and their degradation of a historic building in the largest metropolitan area in Latin America. *Chemosphere* **2021**, *277*, 130286. [CrossRef]
50. Rovira, J.; Nadal, M.; Schuhmacher, M.; Domingo, J.L. Environmental impact and human health risks of air pollutants near a large chemical/petrochemical complex: Case study in Tarragona, Spain. *Sci. Total Environ.* **2021**, *787*, 1–12. [CrossRef]
51. Ly, A.; Cornelisse, J. How to Train a Machine Learning Model in JASP: Clustering, 2019. Available online: https://jasp-stats.org/2019/11/19/how-to-train-a-machine-learning-model-in-jasp-clustering/ (accessed on 28 August 2022).
52. Lee, Y.L.; Makam, S.; McKelvey, S.; Lu, M.W. Durability Reliability Demonstration Test Methods. *Procedia Eng.* **2015**, *133*, 31–59. [CrossRef]
53. Moustafa, K.; Hu, Z.; Mourelatos, Z.P.; Baseski, I.; Majcher, M. System reliability analysis using component-level and system-level accelerated life testing. *Reliab. Eng. Syst.* **2021**, *214*, 107755. [CrossRef]
54. Sánchez-Piñero, J.; Novo-Quiza, N.; Moreda-Piñeiro, J.; Turnes-Carou, I.; Muniategui-Lorenzo, S.; López-Mahía, P. Multi-class organic pollutants in atmospheric particulate matter ($PM_{2.5}$) from a Southwestern Europe industrial area: Levels, sources and human health risk. *Environ. Res.* **2022**, *214*, 114195. [CrossRef] [PubMed]
55. Tong, Y.; Zhao, X.; Li, H.; Pei, Y.; Ma, P.; You, J. Using homing pigeons to monitor atmospheric organic pollutants in a city heavily involving in coal mining industry. *Chemosphere* **2022**, *307*, 135679. [CrossRef]
56. Cui, Y.; Zhang, G.; Wang, W.; Shen, Y.; Zhai, X.; Wu, X.; Li, R.; Wu, B.; Xue, Y. Ten-year emission characteristics of atmospheric pollutants from incineration of sacrificial offerings in China. *Res. J. Environ. Sci.* **2022**, *114*, 391–400. [CrossRef] [PubMed]
57. Guo, X.; Li, S.; Zhang, Y.; Wu, B.; Guo, W. Applications of dynamic simulation for source analysis of soil pollutants based on atmospheric diffusion and deposition model. *Sci. Total Environ.* **2022**, *839*, 156057. [CrossRef]
58. Dong, J.; Wang, X.; Li, J.; Hao, C.; Jiao, L. The Spatial-Temporal Differentiation of Aerosol Optical Properties and Types in the Beijing–Tianjin–Hebei Region Based on the Ecological Functional Zones. *Sustainability* **2022**, *14*, 12656. [CrossRef]
59. Yan, C.; Wang, L.; Zhang, Q. Study on Coupled Relationship between Urban Air Quality and Land Use in Lanzhou, China. *Sustainability* **2021**, *13*, 7724. [CrossRef]
60. Pilarczyk, B.; Tomza-Marciniak, A.; Pilarczyk, R.; Udała, J.; Kruzhel, B.; Ligocki, M. Content of essential and non-essential elements in wild animals from western Ukraine and the health risks associated with meat and liver consumption. *Chemosphere* **2020**, *244*, 125506. [CrossRef] [PubMed]
61. Vystavna, Y.; Huneau, F.; Schäfer, J.; Motelica-Heino, M.; Blanc, G.; Larrose, A.; Vergeles, Y.; Diadin, D.; Le Coustumer, P. Distribution of trace elements in waters and sediments of the Seversky Donets transboundary watershed (Kharkiv region, Eastern Ukraine). *Appl. Geochem.* **2012**, *27*, 2077–2087. [CrossRef]
62. Labunska, I.; Levchuk, S.; Kashparov, V.; Holiaka, D.; Yoschenko, L.; Santillo, D.; Johnston, P. Current radiological situation in areas of Ukraine contaminated by the Chornobyl accident: Part 2. Strontium-90 transfer to culinary grains and forest woods from soils of Ivankiv district. *Environ. Int.* **2021**, *146*, 106282. [CrossRef]
63. Maloshtan, I.; Polishchuk, S.; Kashparov, V.; Yoschenko, V. Assessment of radiological efficiency of countermeasures on peat-bog soils of Ukrainian Polissya. *J. Environ. Radioact.* **2017**, *175–176*, 52–59. [CrossRef]

64. Poursanidis, D.; Traganos, D.; Reinartz, P.; Chrysoulakis, N. On the use of Sentinel-2 for coastal habitat mapping and satellite-derived bathymetry estimation using downscaled coastal aerosol band. *Int. J. Appl. Earth Obs. Geoinf.* **2019**, *80*, 58–70. [CrossRef]
65. Butz, A.; Galli, A.; Hasekamp, O.; Landgraf, J.; Tol, P.; Aben, I. TROPOMI aboard Sentinel-5 Precursor: Prospective performance of CH4 retrievals for aerosol and cirrus loaded atmospheres. *Remote Sens. Environ.* **2012**, *120*, 267–276. [CrossRef]
66. Yang, Y.; Chen, Y.; Yang, K.; Cermak, J.; Chen, Y. High-resolution aerosol retrieval over urban areas using sentinel-2 data. *Atmos. Res.* **2021**, *264*, 105829. [CrossRef]